# The influence of construction parameters and the type of substrate on the conductivity value of multilayer structures made of NiFe and SiO$_2$

Aleksandra Wilczyńska

*Abstract*—**This article presents a method of obtaining multilayer NiFe-SiO$_2$ nanocomposites by non-reactive magnetron sputtering. Structures with different numbers and thicknesses of layers were made on two different types of dielectric substrates. Electrical parameters were tested in the frequency range from 4 Hz to 8 MHz, as well as measurements of the surface roughness of the substrates. Based on the results, the influence of design parameters and the aging effect on the AC properties of the structures was determined.**

*Keywords*—**multilayer nanocomposites; magnetron sputtering; AC measurements; surface roughness**

## I. INTRODUCTION

IN the field of modern electronics, the pursuit of improving device performance while simultaneously minimizing size and energy consumption remains a key challenge. Multilayer structures, especially those composed of permalloy (81% Ni and 19% Fe) and silicon dioxide (SiO$_2$), have garnered significant attention due to their promising electrical properties and potential applications in various fields, including microelectronics and sensor technologies [1,2]. The conductivity of such structures is a crucial parameter influencing their functionality and overall effectiveness in electronic devices. However, understanding the complex interaction between design parameters and substrate type is essential for optimizing their conductivity and, consequently, their performance [3,4]. High-power density dielectric materials play a crucial role in power systems. Unlike other energy storage devices, capacitors constructed from non-conductive materials accumulate and release electrical energy through the process of polarization or depolarization of dipoles in dielectric materials [5]. To date, magnetic nanoparticles have become the focus of researchers due to their unique physicochemical properties and wide range of potential applications. Among the reported applications are magnetic data storage and utilization as a magnetic field sensor, and even as an electrocatalyst in the HER reaction [6,7]. In the field of electronics and functional materials, SiO$_2$ nanocomposites are used as dielectrics with special electrical properties, magnetic insulators or components of highly sensitive sensors, also used in the pharmaceutical industry [8]. Their nanometric structure allows for the control of electrical, thermal conductivity and magnetic properties, which makes them an attractive material for advanced electronic devices [9,10]. These types of structures are often analysed using percolation models, which describe electrical conductivity between particles of metallic materials. The transition from insulator to conductor in metal-dielectric composites is regulated by the volume ratio of the conductive material, where below a certain threshold ($x_c$) the electron tunnelling mechanism or their hopping between grains occurs. Upon reaching this threshold, the Metal-Insulator Transition (MIT) occurs, which influences the electrical properties of the nanocomposite. Once this threshold is surpassed ($x_c < x$), percolation channels form from conductor grains, leading to a change in conductivity type to metallic [11,12].

Nickel and iron are used in the production of alloys such as nickel alloys, stainless steel, etc. Over time, materials may age, which may affect their mechanical and chemical properties. As for iron, it can corrode, especially in the presence of moisture and oxygen. This means that it can rust, forming iron oxides and hydroxides [13]. However, nickel may undergo chemical reactions over time, for example by creating nitrate compounds. Alloys such as NiFe will find very wide application in materials technology. Also, their oxidized forms are often desirable materials. Therefore, in many cases the aging process is accelerated to obtain the expected properties [14-18].

## II. PREPARATION OF MULTILAYER NiFe-SiO$_2$ NANOCOMPOSITES

In this article, we present research on structures obtained through magnetron sputtering. This is a process in which thin layers of material are sputtered onto substrates by bombarding the material source with argon ions, leading to the emission of atoms or ions from the target. These atoms are then deposited onto the substrate surface, forming the desired structure. This method offers many advantages, including high consistency in chemical composition compared to the source material, control over layer thickness, and the ability to deposit various materials,

Aleksandra Wilczyńska is with Faculty of Electrical Engineering and Computer Science, Lublin University of Technology, Lublin, Poland (aleksandra.wilczynska@pollub.edu.pl).

making it an attractive option in the production of advanced materials and devices [19].

Before commencing the fabrication of nanolayers, it was necessary to plan the entire experiment. For this purpose, the Taguchi optimization method was employed. The main objective of using this method was to enhance the production process. The primary aim is to minimize sensitivity to input signal variability to effectively control output variables in the face of random fluctuations. Fundamental concepts in the Taguchi method include loss functions, signal-to-noise ratio (S/N) quality functions, and orthogonal arrays [20]. Considering that certain parameters need to be defined for the discussed method, in my experiment, these were the thicknesses and quantities of layers as independent variables, while the dependent variables were the content of the metallic phase ≤50% of the total volume of the system, aiming not to exceed the percolation threshold [21].
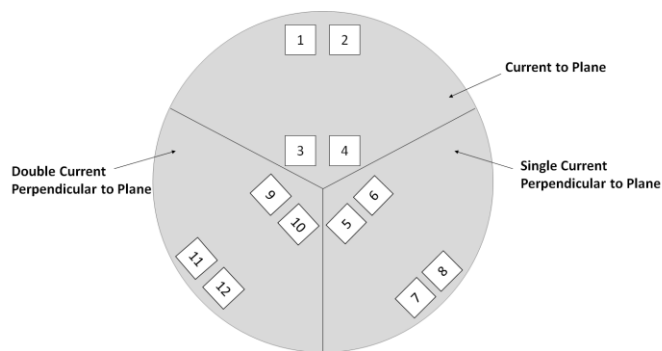


Fig. 1. Structure distribution on the rotating plate in a sputtering machine

To obtain multilayer nanocomposites, the magnetron sputtering method was used using a KJ Lesker 36™ sputtering machine. The first stage was to clean the dielectric substrates (glass and $Al_2O_3$) in an ultrasonic cleaner and polypropylene alcohol. Then they were mounted on a rotating plate and previously designed technological masks were applied to them, which made it possible to obtain structures with repeatable dimensions. The first step was to cover 1/3 of the substrates and sputter a 100 nm copper layer on the rest, which will be used as the bottom contact. Then 1/3 of each metallization layer was covered on one side or in the middle with kapton tape and the entire plate was exposed. The next stage was to initiate the process of spraying the target materials. In series 1 of the structures, 14 layers of 1 nm thickness were alternately sputtered, and in series 2: 10 layers of 2 nm thickness. The layer thicknesses were estimated based on a quartz sensor placed in the vacuum chamber of the sputtering machine. NiFe and $SiO_2$ were selected as the source materials. Contacts enabling measurements were made using silver paste. Structures were obtained in three measurement configurations, i.e. on the surface (CIP-Current to plane), through (CPP-Current perpendicular to plane) and double through (CPP'). Figure 1 shows the distribution of the structures tested. The markings (1,2…12) will be used later in the article. Structures marked with odd numbers were sputtered on laboratory glass, while those with even numbers were sputtered on $Al_2O_3$. Figure 2 shows diagrams with the dimensions of the structures in three measurement configurations.
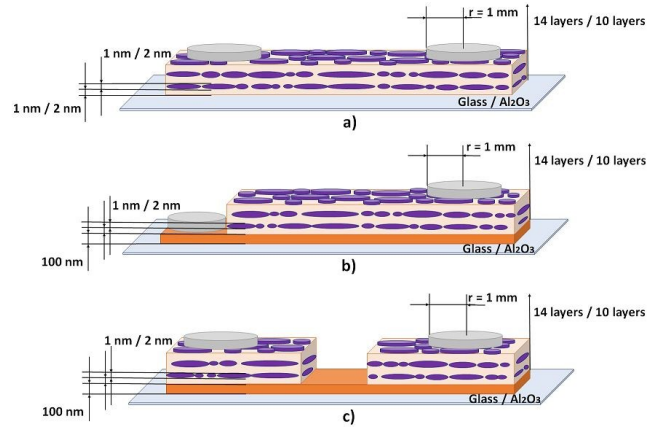


Fig. 2. Dimensions of structures in three measurement configurations: a) current to plane (CIP), b) current perpendicular to plane (CPP), double current perpendicular to plane (CPP')

## III. AC MEASUREMENTS AND CONDUCTIVITY VALUES

The hopping mechanism of electrical conduction effectively describes both DC and AC conduction. This model refers to structures in which grains of conductive material are randomly dispersed in a dielectric matrix. It is based on quantum phenomena such as tunnelling or jumping of electrons between adjacent metal grains, which create neutral potential wells [22]. The mechanism can be divided into three stages. In the first case, neutral potential wells are created in the process of obtaining a nanocomposite. In the second stage, the electron located in the neutral potential well jumps to the neighbouring well under the influence of an external electric field. However, in the third stage, the electron can jump to the next well or return to the previous one. The mechanism in question arises as a result of meeting certain conditions. The first effect is the creation of an alternating electric field (see equation 1), which leads to the creation of a current of tunnelling electrons, described by formula 2, with a specific density.

$$E = E_0 \cdot \sin \omega t \qquad (1)$$

where: $\omega$ – angular frequency, $E_0$ – electric field amplitude, $t$ – time.

$$j = E \cdot \sigma \qquad (2)$$

where: $\sigma$ – material conductivity.

The electron hopping between the wells generates an electric dipole, which leads to the formation of a thermally activated polarization of the material. This process results in an increase in dielectric permittivity. After the negatively charged charge jumps, it remains in the well for some time. There is then a certain probability that this charge will jump to the next well or return to the previous one [23].

The obtained structures underwent characterization of variable current parameters over a frequency range from 4 Hz to 8 MHz using the 4-point method with a Hioki 3536 impedance meter. Due to the aim of comparing technological parameters for research purposes, structures with different numbers and thicknesses of layers were selected for examination. These structures were obtained on two types of substrates with different roughness and in three different measurement configurations, also placed at various positions on the sputtering platter. The distance between the substrate and the sputtering source may affect the repeatability of deposited layers.

Additionally, the aging effect of the structures was investigated one year after fabrication, considering the use of ferromagnetic materials prone to oxidation in atmospheric air and at room temperature. The conductivity of the tested samples was determined based on resistance measurements ($R_p$) and mathematical calculations. Using formula 3, conductivity was calculated for structures in the CIP measurement configuration, while formula 4 was utilized for structures in the CPP and CPP' measurement configurations.

$$\sigma = \frac{\frac{1}{R_p} \cdot l}{S} \left[ S/m \right] \quad (3)$$

where: l – sample length, S – sample surface area.

$$\sigma = \frac{\frac{1}{R_p} \cdot h}{\pi r^2} \left[ S/m \right] \quad (4)$$

where: h – sample thickness, r – contact surface radius.

Figure 3 shows the conductivity versus frequency dependences of structures whose single layer thickness is 1 nm and their number is 14. The presented measurements were made immediately after receipt. In the case of the CIP configuration (Fig. 3a), measurements taken from 120 Hz are presented, because in the low frequency range the resistance values were beyond the meter's range. The same situation was observed in further measurements of structures obtained in this configuration. As can be seen, the conductivity value increases linearly by 5 orders of magnitude with increasing frequency, which excludes mechanical conductivity in the tested material. Measurement values are comparable regardless of the type of substrate on which they were obtained and the distance from the material source. In the case of measurements of the structure in the "through" configuration shown in Figure 3b, it can be seen that the conductivity is constant with increasing temperature in the case of structures obtained on a glass substrate. The value of structure 5, i.e. located in the centre of the plate, is slightly higher than in the case of the structure located on the edge

(structure no. 7). Therefore, its resistance value is lower, which may mean that the layers of conductive material are more continuous. A constant conductivity value indicates that the percolation threshold has probably been exceeded, and thus metallic conductivity. When a certain level that allows electrical conduction is exceeded, paths composed of densely arranged nanoparticles are formed in the nanocomposite. In such a situation, the electrical resistance of the nanocomposite (marked as R) consists of the resistance of the nanoparticles that create the percolation path and the contact resistance between them [24]. What was presented on formula 5.

$$R = \sum_{i}^{n} (R_i + R_C) \left[ R \right] \quad (5)$$

where: $R_i$ – nanograin resistance, $R_C$ – contact resistance.

$$W \approx \exp \left[ -\frac{2}{\hbar} \int_{0}^{d} \sqrt{2m(U(x) - E_e)dx} \quad (6) \right.$$

where: $m$ – electron charge, $d$ – barrier width $E_e$ – kinetic energy of the electron.

However, in structure number 6, which was located in the centre of the plate in the frequency range $<10^6$ Hz, the conductivity value is lower than in the case of structure number 8 and its value is constant up to the frequency of 150 Hz. However, in this case two-step changes can be observed. The first increase in conductivity is observed in the range from 150 Hz to 1.3 kHz, and the next one from 11 kHz. Figure 3c shows the conductivity-frequency dependence of structures in the "double through" (CPP') configuration. Based on the graph, it can be seen that the dependencies of the samples obtained on glass (9 and 11) have the same curves as in the previous case, but their values are slightly smaller, which may be caused by the need to flow the current through a double number of layers (i.e. 28 layers). The patterns of structures on $Al_2O_3$ are more similar to each other than in the case of 14-layers, but electron tunnelling between NiFe grains also occurs in them.
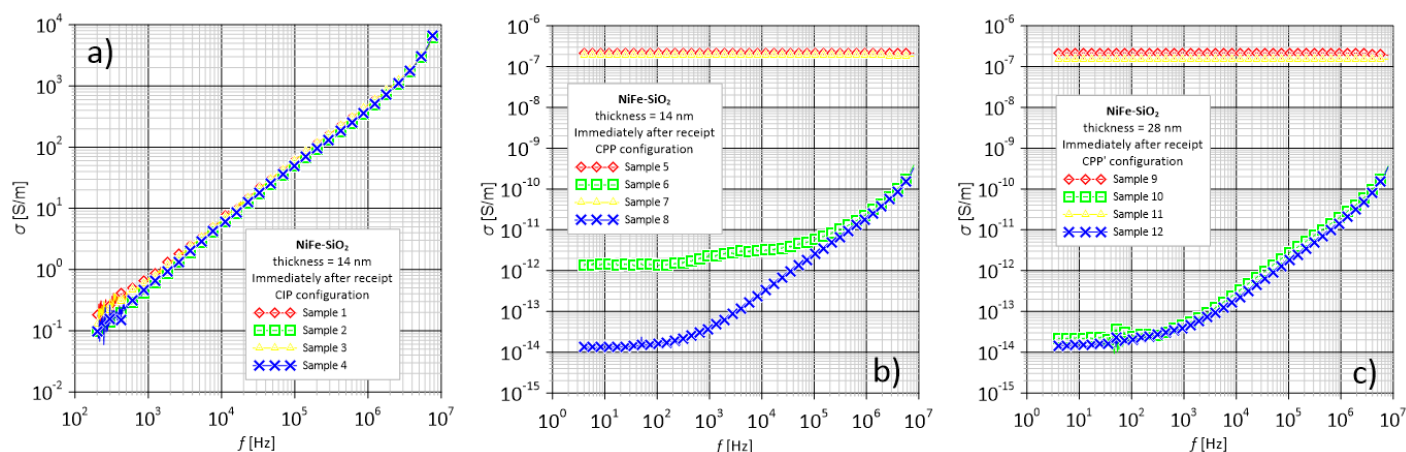


Fig. 3. Dimensions of structures in three measurement configurations: a) current to plane (CIP), b) current perpendicular to plane (CPP), double current perpendicular to plane (CPP').

In Figure 4, measurements of series 1 structures (with a single layer thickness of 1 nm) taken approximately one year after receipt are presented. As can be seen in the graph of structures in the CIP configuration (Fig. 4a), the curves of individual samples practically completely overlap, and their values remain practically unchanged compared to the graphs from measurements immediately after receipt. Based on these results, the repeatability of the parameters of the obtained materials can

be confirmed. Figure 4b shows that in the structure with the CPP configuration, in all tested samples, there was a decrease in the conductivity value, which is caused by the oxidation of metal grains and thus an increase in the diffusion barrier. However, in the case of samples sprayed on laboratory glassware, the oxidation process will not affect the conductivity enough to change the conductivity from the metallic to the dielectric type.

However, significant changes occurred in sample number 6, in which the conduction mechanism changed from a two-step to a single-step conduction mechanism, but can now be adapted to the hopping conduction mechanism of. Mott model, as in the case of sample 8. Also, slight changes were observed in the structures sputtered on $Al_2O_3$ in the CPP' configuration (Fig. 4c).
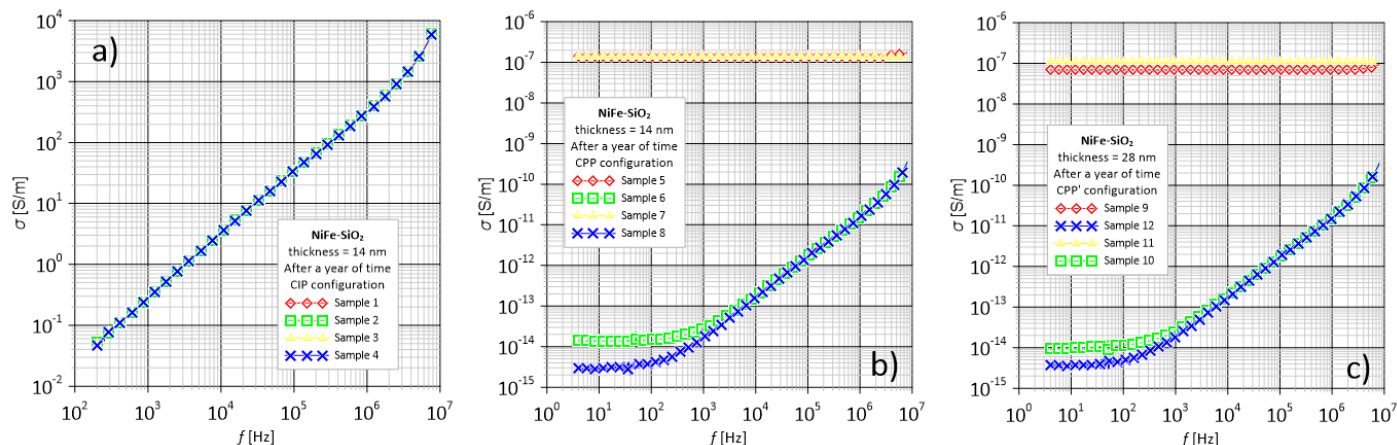


Fig. 4. The dependence of the conductivity on the frequency of structures with a thickness of 14/28 nm after one year in three measurement configurations:
a) CIP, b) CPP, c) CPP'

However, in this case it was observed that in structures sprayed on glass, the oxidation process is more noticeable in the sample located in the centre of the plate, i.e. it rotates around its axis (number 9). It is possible that there are slightly thicker layers in them, and therefore the ratio of its surface to volume in metals decreases. This means there is less space for oxygen to act on per unit volume of metal. It takes longer to reach the inner areas of the metal, which in turn leads to faster oxidation on the outer surfaces. An important observation is the fact that in the case of structures obtained on $Al_2O_3$ in through-through configurations, regardless of the distance from the sputtering source, there is always a hopping or tunnel conduction mechanism. This means that the conductivity in the tested structures is of the dielectric type. Taking into account that the AC parameters are different for different substrates, it can be concluded that this is probably due to the non-smooth surface of $Al_2O_3$. Surface roughness can influence the interfacial interactions between nanomaterials and the substrate. These interactions may influence the dynamics of grain growth and lead to differences in their distribution.

Further tests of AC parameters were carried out on samples in which NiFe and $SiO_2$ layers were alternately sputtered 10 times with 1 nm layers. The conductivity versus frequency relationships shown in Figure 5 represent the structures in question. As can be seen in Figure 5a, the characteristics are comparable to those of the previous series of structures. Only sample 4 located on the edge of the plate and obtained on an $Al_2O_3$ substrate shows slightly lower conductivity values throughout the entire frequency range compared to the rest of the samples. A completely different situation was observed in cross-configuration structures (Fig. 5b). In this case, a constant conductivity value was observed in all tested samples over the entire frequency range. Only slight increases in the high

frequency range may indicate the occurrence of the current skin phenomenon. Samples number 5 and 7 (obtained on glass) have very similar values. The structure located in the middle has slightly higher conductivity and therefore lower resistance. On this basis, it can be concluded that the current flows more freely through such a material, which may be due to slightly thicker and thus more uniform layers. Metallic type conductivity is also observed in samples prepared on $Al_2O_3$. The graph shows that sample 8 has a conductivity value that is almost one order of magnitude lower than sample number 6. This may be due to the fact that the CPP' sample located on the edge of the turntable does not rotate around its axis as the samples do. located in its centre, and therefore it is possible that less material was deposited on the substrates. This means that the layers are thinner, and consequently, the conducting material islands are further apart. Completely different relationships can be observed in structures where the current flows through 20 layers (as if through 40 nm of material) as depicted in Figure 5c. In contrast to the previous series, a constant conductivity value, followed by an almost linear increase with frequency, is observed in samples obtained on laboratory glass (9 and 11). In sample number 11, a conductivity value jump occurs in the frequency range from 10 Hz to approximately 80 Hz, which is attributed to a bridge jumping in the impedance meter and does not affect the conduction mechanism in the investigated structure. On the other hand, structures obtained on $Al_2O_3$ exhibit constant conductivity values, which may indicate exceeding the percolation threshold of the system. Additionally, comparing samples in single and double through configuration measurement, it can be observed that conductivity decreases by an order of magnitude with an increase in the number of layers. This suggests that an increase in structure thickness may lead to an increase in resistance of the investigated nanocomposite.
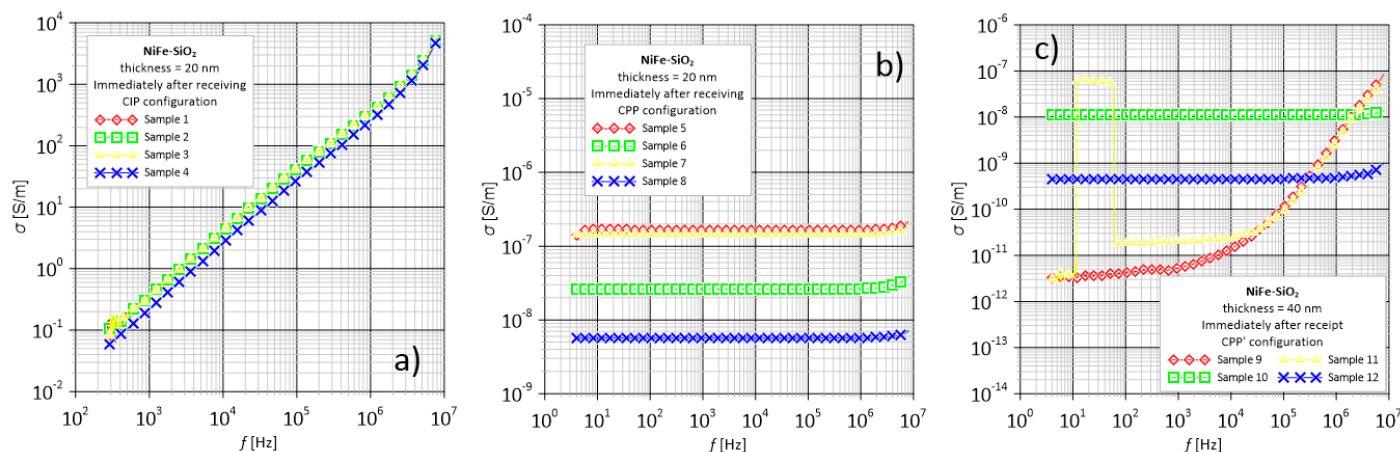
Fig. 5. The dependence of the conductivity on the frequency of structures with a thickness of 10/20 nm after one year in three measurement configurations: a) CIP, b) CPP, c) CPP'.

Figure 6 shows measurements of the same series performed after a year. Oxidation of grains in samples with the CIP configuration resulted in repeatability of the conductivity values of all samples (Fig. 6a). Exactly the same situation could be observed in the structures shown in Figure 4a. In turn, some changes occurred in samples 7 and 8 (Fig. 6b). In structure no. 7, during the measurements, the bridge in the meter jumped at a frequency of 3 kHz. From this value, the conductivity value begins to increase by 3 orders of magnitude. However, it cannot be clearly said that the conduction mechanism has changed in the structure under study by oxidation. It may also be the occurrence of the accumulation of electric charge on the sample surface. An interesting situation can be observed in sample number 8. In this case, after a year, the conductivity value decreased by more than 1 order of magnitude. The oxidation process often leads to a change in the chemical structure of a substance. As a result, this change may lead to a decrease in conductivity. Another possible reason is that the samples were stored in housings where they could be damaged. The oxidation process can also damage the structure of the material, for example by creating cracks or defects. These damages can disturb the flow of current through the material, which leads to a reduction in its conductivity. Figure 6c shows the measurement of the structure in the CPP' configuration. The aging process in the sample located in the centre of the plate and obtained on an $Al_2O_3$ substrate (no. 10) caused a slight decrease in the conductivity value. In sample number 11, immediately after receipt, an increase in conductivity was observed from the value of 10 kHz. However, measurements carried out after a year showed that the increase was shifted to the lower frequencies (from 1 kHz). Significant changes occurred in sample number 9 obtained on glass. In this case, from one hopping conduction mechanism, the oxidation process gave rise to three mechanisms. One in the frequency range of 1 kHz-40 kHz, the second in the range of 40 kHz-1 MHz, and the third in the range of 1 MHz-8 MHz. In turn, in structure number 12, which was located on the edge of the plate and was obtained on an $Al_2O_3$ substrate, the aging process caused the oxidation of metal grains/layers, thereby increasing the diffusion barriers around them, which results in a change in conductivity from a typically metallic to a tunnel conduction mechanism, i.e. dielectric type.
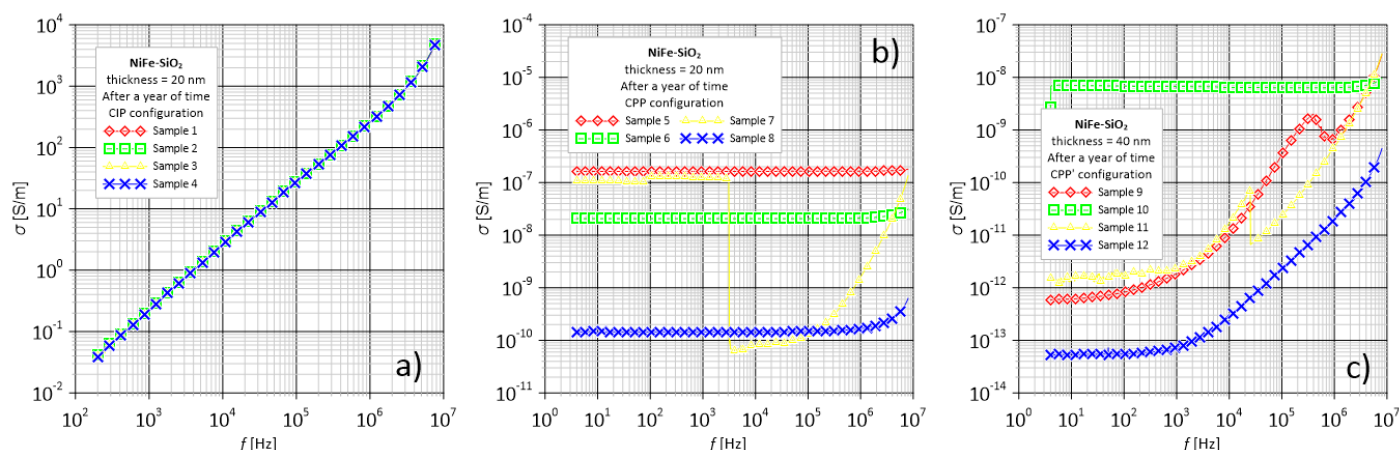


Fig. 6. The dependence of the conductivity on the frequency of structures with a thickness of 10/20 nm after one year in three measurement configurations: a) CIP, b) CPP, c) CPP'.

## IV. SURFACE ROUGHNESS MEASUREMENTS OF SUBSTRATES

As previously mentioned, the type of substrate affects the alternating current properties of multilayer nanocomposites. Therefore, the roughness profiles of the glass and $Al_2O_3$ substrate were investigated. The tests were carried out using a Taylor Hobson profilemeter in accordance with the ISO 4287 standard. Parameters such as maximum peak height of the roughness profile (Rp), maximum valley depth of the roughness profile (Ry), maximum height of the roughness profile (Rz), average height of roughness profile elements (Rc), total height of the roughness profile (Rt), arithmetic mean deviation of the roughness profile (Ra), root mean square deviation of the roughness profile (Rq), asymmetry of the roughness profile (Rsk), kurtosis of the roughness profile (Rku) were measured 10 times. As can be seen, the glass values are much lower than those of the oxide substrate. This may have a significant impact on the accumulation of metal grains in the dielectric matrix. Additionally, $Fe_3O_4$ nanoparticles are characterized by a significant volume-to-surface ratio, which leads to high surface energy, which in turn promotes particle aggregation. Moreover, $Fe_3O_4$ has high chemical activity on its surface, which makes it susceptible to oxidation in contact with air [6]. Table 1 presents the amplitude parameters.

TABLE I
AMPLITUDE PARAMETERS – ROUGHNESS PROFILE

|          | Glass  | $Al_2O_3$ |
|----------|--------|-----------|
| Rp, μm   | 0.02   | 2.92      |
| Rv, μm   | 0.01   | 4.24      |
| Rz, μm   | 0.06   | 7.17      |
| Rc, μm   | 0.00   | 2.94      |
| Rt, μm   | 0.12   | 8.81      |
| Ra, μm   | 0.009  | 1.08      |
| Rq, μm   | 0.01   | 1.33      |
| Rsk, -   | 1.782  | -0.443    |
| Rku, -   | 10.098 | 3.04      |

## CONCLUSION

The paper presents the entire sequence of technological processes aimed at obtaining multilayer nanocomposites made of NiFe and SiO2 by dual-source magnetron sputtering on two different types of non-conductive substrates, i.e. laboratory glass and $Al_2O_3$, as well as with different single layer thicknesses. Additionally, thanks to the use of a technological mask, structures were created that could be measured in three different configurations: on the surface, through and twice through. Measurements were carried out immediately after receipt and then after approximately one year to determine the aging effect on the AC properties of the structures. In the case of samples with the CIP measurement configuration, there was no influence of the number and thickness of layers, and no changes resulting from long-term storage in the presence of an air atmosphere were observed. However, noticeable changes occur in series 1 structures in through-through measurement configurations. The roughness of the $Al_2O_3$ substrate surface probably caused the ferromagnetic grains to accumulate into larger clusters, which caused a change in the type of conduction, which is characteristic of the hopping/tunnel conduction mechanism. After some time, it was found that the oxidation of the metal grains slightly influenced the parameters of the

structures on the oxide substrate and no changes were observed in the structures obtained on the glass. A very similar situation can be seen in the case of series 2 samples, where the thickness of a single layer is 2 nm. In this case, the through-through measurement configuration, and thus the doubling of the number of layers, as well as the aging effect significantly affect the electrical properties of the nanocomposites. Not only causing changes in the conduction type from metallic to dielectric, but also increasing the number of conduction mechanisms.

Based on the results obtained, it can be concluded that the design parameters as well as the oxidation of ferromagnetic grains in the aging process have a significant impact on the AC properties of multilayer NiFe-SiO2 nanocomposites.

## REFERENCES

[1] Tan, X., Huang, D., Zhao, M., Cheng, Q., Ren, Y., Chen, Y., Ren, Y., Cheb, Y., Yi, M., Zuo, X., Wang, Y., Song, Y., Lu. Q., Han, G., Li, H., "Research about passivation layer of SiO2 in GMR sensors for magnetic bead detection", Journal of Magnetism and Magnetic Materials, vol. 585, 170912, 2023. https://doi.org/10.1016/j.jmmm.2023.170912

[2] Baig, M. M., Pervaiz, E., Azad, M., Jahan, Z., Niazi, M. B. K., Baig, S. M., "NiFe2O4/SiO2 nanostructures as a potential electrode material for high rated supercapacitors", Ceramics International, vol. 47, no. 9, pp. 12557-12566, 2021. https://doi.org/10.1016/j.ceramint.2021.01.113

[3] Brautman L.J., Krock R.H., "Composite Materials", Academic Press, New York, 1975

[4] Fedotov, A. K., Pashkevich, A. V., Fedotova, J. A., Fedotov, A. S., Kołtunowicz, T. N., Zukowski, P., Ronassi, A. A., Fedotova, V. V., Svito, I. A., Budzyński, M., "Electron transport and thermoelectric properties of ZnO ceramics doped with Fe", Journal of Alloys and Compounds, vol. 854 2021, 156169, 2021. https://doi.org/10.1016/j.jallcom.2020.156169

[5] Jiang J., Shen, Z., Qian, J., Dan, Z., Guo, M., Lin, Y., Nan, C-W., Chen, L., Shen, Y., "Ultrahigh discharge efficiency in multilayered polymer nanocomposites of high energy density", Energy Storage Materials, vol. 18, pp. 213-221, 2019. https://doi.org/10.1016/j.ensm.2018.09.013

[6] Nikmah A., Taufiq, A., & Hidayat, A., "Synthesis and characterization of Fe3O4/SiO2 nanocomposites", Earth and Environmental Science, vol. 276, 012046, 2019. https://doi.org/10.1088/1755-1315/276/1/012046

[7] Ali Z., Mehmood, M., & Ghazi, Z. A., "Herring bone graphitic nanofibers grown on NiFe-silica nanocomposites by CVD method for HER activity in alkaline media", Materials Letters, vol. 305, 130838, 2021. https://doi.org/10.1016/j.matlet.2021.130838

[8] Sciuto E.L., Bongiorno, C., Scandurra, A., Petralia, S., Cosentino, T., Conoci, S., Sinatra, F., Libertino, S., "Functionalization of bulk SiO2 surface with biomolecules for sensing applications: Structural and functional characterizations", Chemosensors, vol. 6, no. 4, 2018. https://doi.org/10.3390/chemosensors6040059

[9] Zukowski P., Koltunowicz, T. N., Bondariev, V., Fedotov, A. K., Fedotova, J. A., "Determining the percolation threshold for $(FeCoZr)_x(CaF_2)_{(100-x)}$ nanocomposites produced by pure argon ion-beam sputtering", Journal of Alloys and Compounds, vol. 683, pp. 62-66, 2016. https://doi.org/10.1016/j.jallcom.2016.05.070

[10] Zhu W., Zheng, G., Cao, S., He, H., "Thermal conductivity of amorphous SiO2 thin film: A molecular dynamics study", Scientific reports, vol. 8, 10537, 2018, https://doi.org/10.1038/s41598-018-28925-6

[11] Raquet B., Goiran, M., Negre, N., Leotin, J., Aronzon, B., Rylkov, V., Meilikhov, E., "Quantum Size Effect transition in percolating nanocomposite films", Phys. Rev., vol. 62, 17144, 2000

[12] Clerc J.P., Giraud, G., Laugier, J. M., Luck, J. M., "The electrical conductivity of binary disordered systems, percolation clusters, fractals and related models", Advances in Physics, vol. 39, pp. 191-309, 1990. https://doi.org/10.1080/00018739000101501

[13] Du, S., Ren, Z., Wang, X., Wu, J., Meng, H., Fu, H., "Controlled Atmosphere Corrosion Engineering toward Inhomogeneous NiFe-LDH for Energetic Oxygen Evolution", ACS Nano, vol. 16, no. 5, 7794–7803, 2022. https://doi.org/10.1021/acsnano.2c00332

[14] Navadeepthy D., Thangapandian, M., Viswanathan, C., & Ponpandian, N., "A nanocomposite of $NiFe_2O_4$–PANI as a duo active electrocatalyst toward the sensitive colorimetric and electrochemical sensing of ascorbic acid", Nanoscale Adv., vol. 2, pp. 3481-3493, 2020. https://doi.org/10.1039/D0NA00283F

[15] Tian Y. Z., Yang, Y., Peng, S. Y., Pang, X. Y., Li, S., Jiang, M., Li, M. X., Wang, J. W., Qin, G. W., "Managing mechanical and electrical properties of nanostructured Cu-Fe composite by aging treatment", Materials Characterization, vol. 196, 112600, 2023. https://doi.org/10.1016/j.matchar.2022.112600

[16] Tsoi G. M., Wenger, L. E., Senaratne, U., Tackett, R. J., Buc, E. C., Naik, R., Waishnava, P. P., Naik, V., "Memory effects in a superparamagnetic $\gamma-Fe_2O_3$ system", Phys. Rev. B, vol. 72, 014445, 2005. https://doi.org/10.1103/PhysRevB.72.014445

[17] Islam, R. A., Priya, S, "Synthesis of High Magnetoelectric Coefficient Composites Using Annealing and Aging Route", Applied Ceramic Technology, vol. 3, no. 5, pp. 353-363, 2006. https://doi.org/10.1111/j.1744-7402.2006.02099.x

[18] Wilczyńska A., Kołtunowicz, T. N., Kociubiński, A., Guzowski, B., Łakomski, M., "Influence of design and annealing parameters on measurements of AC properties of $NiFe-SiO_2$ multilayer structures", Journal of Magnetism and Magnetic Materials, vol. 597, no. 1, 172030, 2024. https://doi.org/10.1016/j.jmmm.2024.172030

[19] Kelly P.J., Arnell R.D., "Magnetron sputtering: a review of recent developments and applications", Vacuum, vol. 56, pp. 159-172, 2000. https://doi.org/10.1016/S0042-207X(99)00189-X

[20] Freddi, A., Salmon, M, "Design principles and methodologies" Cham: Springer, pp. 159-180, 2019. https://doi.org/10.1007/978-3-319-95342-7

[21] Harter T., "Finite-size scaling analysis of percolation in three-dimensional correlated binary Markov chain random fields", Physical Review E, vol. 72, 026120, 2005. https://doi.org/10.1103/PhysRevE.72.026120

[22] Żukowski P., Kołtunowicz, T., Partyka, J., Węgierek, P., Kolasik, M., Larkin, A., Fedotova, J., Fedotov, F., Vlasukova, L. A., „Model przewodności skokowej i jego weryfikacja dla nanostruktur wytwarzanych technikami jonowymi", Przegląd Elektrotechniczny vol. 84, no. 3, pp. 247-249, 2008.

[23] Żukowski P., Koltunowicz, T. N., Boiko, O., Bondariev, V., Czarnacka, K., Fedotova, J. A., Fedotov, A. K., Svito, I. A., "Impedance model of metal dielectric nanocomposites produced by ion-beam sputtering in vacuum conditions and its experimental verification for thin films of $(FeCoZr)_x(PZT)_{(100-x)}$", Vacuum, vol. 120, pp. 37-43, 2015. https://doi.org/10.1016/j.vacuum.2015.04.035

[24] Wilczyńska A., Kociubiński, A., Kołtunowicz, T. N., "Preparation of Discontinuous $Cu/SiO_2$ Multilayers – AC Conduction and Determining the Measurement Uncertainty", Sensors, vol. 23, no. 5, 2842, 2023. https://doi.org/10.3390/s23052842

[25] Raddaoui Z., El Kossi, S., Brahem, R., Bajahzar, A., Valentinovich Trukhanov, A., Leonidovich Kozlovskiy, A., Zdorovets, M. V., Dhahri, J., Belmabrouk, H., "Hopping conduction mechanism and impedance spectroscopy analyses of $La_{0.70}Sr_{0.25}Na_{0.05}Mn_{0.70}Ti_{0.30}O_3$ ceramic", Journal of Materials Science: Materials in Electronics, vol. 32, pp. 16113–16125, 2021. https://doi.org/10.1007/s10854-021-06160-6

[26] Zaafouri A., Gzaiel, M., Gharbi, I., Bakari, B., "Electrical conductivity and hopping conduction mechanism by CBH model in $AgCoPO_4$ compound prepared using solid-state reaction", Journal of Materials Science: Materials in Electronics, vol. 35, pp. 1-12, 2024. https://doi.org/10.1007/s10854-024-12475-x

[27] Bocharov G. S., Eletskii, A. V., "Percolation Conduction of Carbon Nanocomposites, Molecular Sciences", vol. 21, no. 20, 7634, 2020. https://doi.org/10.3390/ijms21207634